

Performance Assessment and Parametric Design of a Combined System Consisting of High-Temperature Proton Exchange Membrane Fuel Cell and Absorption Refrigerator

Yuan Han¹, Xinru Guo¹, Houcheng Zhang^{1,*}, Ziyang Hu¹, Shujin Hou^{2,*}

¹ Department of Microelectronic Science and Engineering, Ningbo University, Ningbo 315211, China

² College of Physics and Electronic Engineering, Nanyang Normal University, Nanyang 473061, China

*E-mail: zhanghoucheng@nbu.edu.cn (H. Zhang); houshujingrb@163.com (S. Hou).

Received: 20 April 2019 / Accepted: 30 June 2019 / Published: 31 July 2019

A theoretical model of a combined system composed of a high-temperature proton exchange membrane fuel cell (HT-PEMFC), a regenerator and an absorption refrigerator (APR) is established, where the APR is used to absorb the waste heat from HT-PEMFC for cooling production. By taking irreversible losses within the proposed system into account, mathematical expressions of the equivalent output power and efficiency for HT-PEMFC, APR and the combined system are derived and the optimum operating regions of system performance parameters are obtained. In addition, the effects of key parameters such as operating temperature, doping level, relative humidity, proton exchange membrane thickness and some composite parameters on the combined system performance are discussed in detail. The obtained results can provide some guidelines for the integration and design of such an actual system.

Keywords: High-temperature proton exchange membrane fuel cell; Absorption Refrigerator; Waste heat recovery; Performance analysis; Parametric design

1. INTRODUCTION

Fuel cells have been hailed as an alternative to conventional fossil fuel power generation technologies because of their high efficiency, zero toxic emissions and potential to reduce the burden of primary energy consumption. Fuel cells have great potential in a wide range of applications, including large-scale fixed generation, scattered cogeneration and portable power sources [1-2]. In a variety of fuel cells, the proton exchange membrane fuel cell (PEMFC) is regarded as one of the most potential clean energy technologies because of its significant advantages such as fast startup, low operating temperature, immediate response ability [1-4]. However, it is reported that up to half of the chemical energy in hydrogen will be eventually dissipated as waste heat in PEMFCs due to the irreversible losses resulting

from electrochemical reactions and joule heat [5]. If the waste heat is not immediately removed, the accumulated heat may affect the normal operation of the PEMFC [3-6]. Therefore, it is of great significance to reuse the waste heat generated from PEMFCs for other applications, as it kills two birds with one stone.

Based on the operating temperature, PEMFCs can be classified into high-temperature PEMFCs (HT-PEMFCs) and low-temperature PEMFCs (LT-PEMFCs). The HT-PEMFCs are a kind of promising technology that may overcome many problems faced in LT-PEMFCs, such as carbon monoxide (CO) poison [7, 8], waste heat removal difficulty and comparatively complicated water management system [9, 10]. In addition, HT-PEMFC does not require a humidifier or CO removal process, so the system configuration of HT-PEMFC is simpler than that of LT-PEMFC [11, 12]. Moreover, HT-PEMFC has a higher operating temperature (120°C~200°C), which greatly simplifies the complexity of HT-PEMFC thermal management [13-15] and provides higher quality thermal energy than LT-PEMFC.

At present, most studies of HT-PEMFCs mainly focus on aspects, such as research and development of cost-effective proton exchange membranes [16], fuel cell configuration optimization [17], electrode structures design [18], high-performance and low-platinum electrocatalysts and multi-platinum alloy catalysts [19], etc. While relatively few studies have been conducted on the waste heat recovery of HT-PEMFC [20, 21]. Perna et al. [22] proposed a HT-PEMFC/organic Rankine cycle cogeneration system for providing power and heat to independent residential utilities, and the maximum electric power and the corresponding electric efficiency were found to be 27 kW and 43%, respectively. Sarabchi et al. [23] studied an electricity/heating cogeneration system composed of a HT-PEMFC, a solar methanol steam reformer and a Kalina cycle, and showed that the average dairy exergy efficiency can increase by up to 29.3.

Absorption refrigerators (APRs) can be thermally activated by industrial waste heat, solar energy, geothermal and other low-grade thermal energy [24], which offer advantages such as reliable, silent and environmentally friendly. To date, many studies have been undertaken to use APRs to recovery the waste heat from PEMFCs [26-32]. For example, Pilatowsky et al. [25] introduced a cogeneration system consisting of a LT-PEMFC and an APR, and the results showed that the cogeneration efficiency reached the maximum value of 28.6%~37.3%. Arsalis [26] put forward a HT-PEMFC/APR combined system and studied the potential of this technology in future applications. Due to the higher operating temperature, HT-PEMFCs are superior to LT-PEMFCs as the topping cycle for APRs. The technology coupling APRs to HT-PEMFCs can be widely used in scenes that electricity and cooling are both needed. For example, Lee et al. [33] proposed a combined system consisting of a HT-PEMFC and an APR to provide both electricity and cooling, and the output electrical efficiency and equivalent power of the combined system were improved by 8% and 24~50% in comparison with the single HT-PEMFC, respectively. However, the effects of various operating conditions and design parameters on the HT-PEMFC/APR combined system performance are still unrevealed. The relative studies may provide some new insights into running and designing such an actual system.

In this work, a HT-PEMFC/APR combined system is proposed to simultaneously produce electricity and cooling. The structure of this paper is organized as follows: In Section 2, each component within the proposed system is mathematically described, and the mathematical expressions for power output and efficiency of the combined system consisting of HT-PEMFC and APR are obtained. In

Section 3, the general performance characteristics of the combined system are demonstrated and the optimum operating ranges for some key performance parameters are given, and the effects of some important parameters on the performance of the combined system are discussed in detail.

2. SYSTEM DESCRIPTION

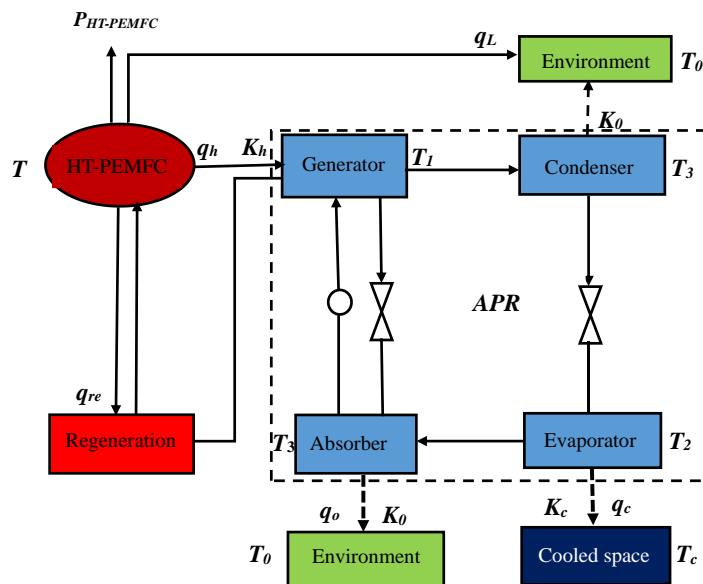


Figure 1. Diagram of the HT-PEMFC/APR combined system.

The proposed combined system comprised of an HT-PEMFC, an APR and a regenerator, where the APR is mainly composed of a generator, an evaporator, an absorber and a condenser. As shown in the Fig. 1, HT-PEMFC generates electrical power $P_{HT-PEMFC}$ and waste heat through electrochemical reactions. The rate of waste heat generated by HT-PEMFC q_h is flowed to the generator at temperature T_1 to drive the APR for cooling purpose; another part q_{re} is flowed to the regenerator to recompense the regeneration losses; and the third part q_L is directly leaked into the ambience [29, 34-36]. q_c is the heat transfer rate of the working fluid from the cooling space at temperature T_c to the evaporator at temperature T_2 . q_0 is the total heat transfer rate of the working fluid from the condenser and the absorber at temperature T_3 to the ambience at temperature T_0 . For this combined system, the waste heat generated by the HT-PEMFC can be readily used by the APR for cooling production without providing any electricity, therefore, the energy conversion efficiency is expected to be further improved.

To facilitate the description of major irreversible losses, some simplified assumptions are made as follows [37-39]:

- Each subsystem within the combined system is operated under stable states;
- Hydrogen and air are supplied according to the generated electric current;
- The working fluid temperature for the absorber and condenser are the same;
- The electrical energy needed to compress hydrogen and air is neglected;

- The working fluid in the APR continuously exchanges heat with the heat reservoirs;
- Heat transfers in the system obey Newton's laws.

2.1. HT-PEMFC

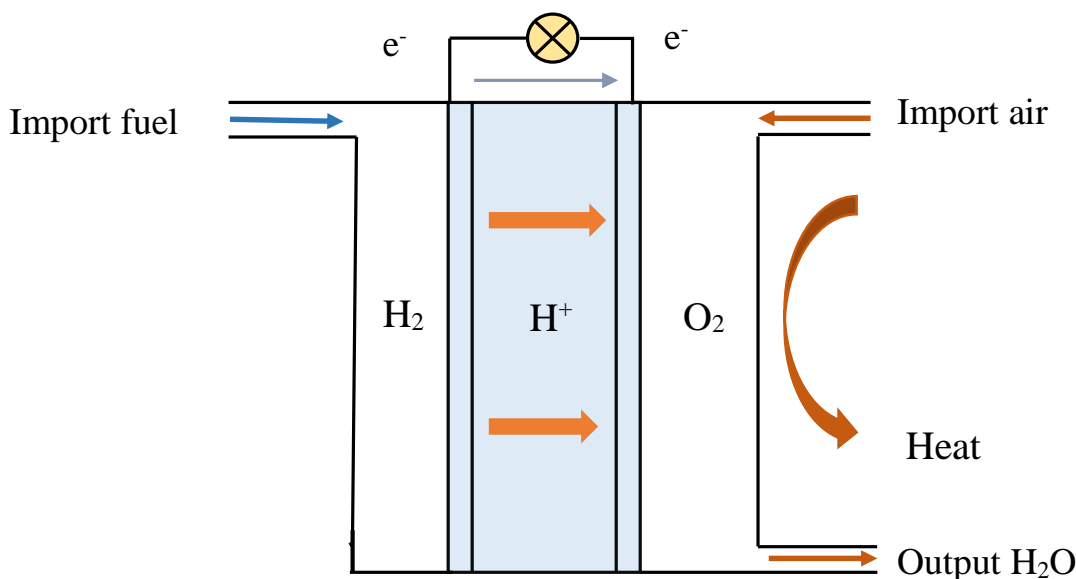


Figure 2. Diagram of an HT-PEMFC.

As shown in Fig. 2, the HT-PEMFC within the hybrid system mainly consists of a cathode and an anode with phosphoric-acid-doped polybenzamidazole ((PBI)/H₃PO₄) membrane as electrolyte between the anode and the cathode. The HT-PEMFC is a power generation device that directly converts the chemical energy stored in H₂ and O₂ into electric energy and thermal energy. H₂ and O₂ reach both sides of the proton exchange membrane through the diffusion layer and the catalytic layer on the electrodes, respectively. On the anode side, H₂ is dissociated into H⁺ and e⁻ under the action of the catalyst. H⁺ is transferred in the proton exchange membrane in the form of water and protons (xH₂O), and finally reaches the cathode to achieve proton conduction. The anodic reaction is expressed as: H₂ → 2H⁺ + 2e⁻. At the same time, O₂ at cathode combines with the H⁺ under the action of the catalyst. The cathodic reaction is expressed as: 2H⁺ + 1/2 O₂ + 2e⁻ → H₂O. The overall electrochemical reactions of HT-PEMFC are: H₂(g) + 1/2 O₂(g) → H₂O(g) + electricity + heat [40-42].

The produced electricity is delivered to the external electric circuit and the produced heat is usually rejected into the ambience without any recovery. Adopting the HT-PEMFC electrochemical model from Refs. [24, 30], the output voltage *U* of a single cell is always lower than the reversible voltage *E*₀ owing to the electrochemical irreversible losses such as activation overpotential (*E*_{act}), concentration overpotential (*E*_{con}) and ohmic overpotential (*E*_{ohm}). As a consequence, the power output *P*_{HT-PEMFC} and efficiency *η*_{HT-PEMFC} of a single HT-PEMFC can be, respectively, given by [37, 38, 43, 44]:

$$P_{HT-PEMFC} = jA(U - E_{act} - E_{con} - E_{ohm}) \tag{1}$$

and

$$\eta_{HT-PEMFC} = \frac{2F}{-\Delta h}(U - E_{act} - E_{con} - E_{ohm}) \tag{2}$$

where j is the operating current density; A is the effective polar plate area of the HT-PEMFC; F is the Faraday's constant, Δh is the molar enthalpy change of the overall electrochemical reactions.

The output voltage U is given by [30, 42]

$$U = E_0 + \frac{\Delta s}{n_e F} + \frac{RT}{n_e F} \ln(p_{H_2} P_{O_2}^{0.5} / p_{H_2O}) \tag{3}$$

where $E_0 = \frac{\Delta g^0}{n_e F}$ is the ideal standard potential, Δg^0 is standard molar Gibbs free energy change of the electrochemical reactions at $T = 298$ K and $P = 1.00$ atm; n_e is the number of electrons exchanged per hydrogen molecule; Δs is the molar entropy change of the electrochemical reactions; R is the universal gas constant; P_{O_2} , P_{H_2} and P_{H_2O} are, respectively, the partial pressures of O_2 , H_2 and H_2O .

The activation overpotential is

$$E_{act} = \frac{RT}{2\alpha F} \ln\left(\frac{j + j_{leak}}{j_0}\right) \tag{4}$$

where α , j_{leak} and j_0 are the charge transfer coefficient, the leakage current density, and the exchange current density, respectively [41, 44].

The concentration overpotential is

$$E_{con} = \left(1 + \frac{1}{a}\right) \frac{RT}{2F} \ln\left(\frac{j_L}{j_L - j}\right) \tag{5}$$

where j_L stands for the limiting current density [43].

The ohmic overpotential can be expressed as

$$E_{ohm} = j \frac{t_{mem}}{\sigma_{mem}} \tag{6}$$

where $\sigma_{mem} = \frac{A_0 B}{T} e^{-\frac{b_{act}}{RT}}$ and t_{mem} are, respectively, the proton conductivity of the electrolyte and the thickness, $A_0 = 168DL^3 - 6324DL^2 + 65750DL + 8460$ and $b_{act} = -619.6DL + 21750$, DL and Rh are the doping level [45-47] and relative humidity of the electrolyte, respectively. The value of B varies with the operating temperature T : when the operating temperature is in the range of $373.15 < T < 413.15$, $B = 1 + (0.01704T - 4.6767)Rh$; when the operating temperature is in the range of $413.15 \leq T \leq 453.15$, $B = 1 + (0.1432T - 56.89)Rh$; when the operating temperature is outside of the ranges mentioned above, $B = 1 + (0.7T - 309.2)Rh$.

2.2. APR

The APR in the combined system is driven by the waste heat generated in HT-PEMFC. Once some of the waste heat of HT-PEMFC flows to the generator, the APR begins to extract heat from the

cooling space [48]. By considering internal irreversible effects inside the working fluids and the external finite-rate heat transfer irreversibilities, the maximum cooling rate of the APR R_0 and its corresponding coefficient of performance ε are, respectively, given by [49-51]:

$$R_0 = q_c = \frac{q_h}{2} \left\{ \left[\left(a + \frac{I_r T_0 - T_c}{Cq_h} \right)^2 - 4T_c \left(\frac{1}{(1+D)^2 T} - \frac{1 - I_r T_0/T}{Cq_h} \right) \right]^{0.5} - \left[a + \frac{I_r T_0 - T_c}{Cq_h} \right] \right\} \quad (7)$$

and

$$\varepsilon = \frac{1}{2} \left\{ \left[\left(a + \frac{I_r T_0 - T_c}{Cq_h} \right)^2 - 4T_c \left(\frac{1}{(1+D)^2 T} - \frac{1 - I_r T_0/T}{Cq_h} \right) \right]^{0.5} - \left[a + \frac{I_r T_0 - T_c}{Cq_h} \right] \right\} \quad (8)$$

where $a = 1 + (T_c - I_r D^2 T_0) / [(1+D)^2 T]$, $D = [b_1^{0.5} - 1] / [1 + (I_r b_1)^{0.5}]$, $b_1 = K_h / K_0$, $b_2 = K_h / K_c$, $C = (1+D)^2 / (A_R K)$, $K = K_h / [1 + \sqrt{I_r b_1}]^2$, I_r is the internal irreversible factor of the working substance, K_h and K_c are, respectively, the heat transfer coefficients of generator and evaporator, K_0 is the heat transfer coefficient of condenser or absorber, $A_R = A_h + A_c + A_0$ is the total heat-transfer area of the APR, A_h and A_c are, respectively, heat transfer areas of generator and evaporator, A_0 is the total heat transfer area of the condenser and absorber.

As the exergy contents of the cooling load and electric power are different, the equivalent power output P_{APR} and efficiency η_{APR} for the APR can be, respectively, given as [50-52]:

$$P_{APR} = \frac{q_h}{2} \left| 1 - \frac{T_0}{T_c} \right| \left\{ \left[\left(a + \frac{I_r T_0 - T_c}{Cq_h} \right)^2 - 4T_c \left(\frac{1}{(1+D)^2 T} - \frac{1 - I_r T_0/T}{Cq_h} \right) \right]^{0.5} - \left(a + \frac{I_r T_0 - T_c}{Cq_h} \right) \right\} \quad (9)$$

and

$$\eta_{APR} = \frac{P_{APR}}{q_h} = \frac{1}{2} \left| 1 - \frac{T_0}{T_c} \right| \left\{ \left[\left(a + \frac{I_r T_0 - T_c}{Cq_h} \right)^2 - 4T_c \left(\frac{1}{(1+D)^2 T} - \frac{1 - I_r T_0/T}{Cq_h} \right) \right]^{0.5} - \left[a + \frac{I_r T_0 - T_c}{Cq_h} \right] \right\} \quad (10)$$

2.3. Regenerator

The regenerator in this system is used as a counter-flow heat exchange, and the rate of regeneration loss q_{re} is usually calculated as follows [6]:

$$q_{re} = K_{re} A_{re} (1 - \varepsilon) (T - T_0) \quad (11)$$

Where K_{re} and A_{re} are, respectively, the heat-transfer coefficient and heat-transfer area of the regenerator.

2.4. Power output and efficiency of the combined system

The rate of heat leaked from the HT-PEMFC to the ambience q_L is usually assumed in proportion to the temperature difference between the HT-PEMFC and the ambience, i.e.,

$$q_L = K_L A_L (T - T_0) \tag{12}$$

Where K_L is the conductive and/or convective heat-leak coefficient, A_L is the corresponding heat-leak area.

According to the energy conservation law, q_h can be given as [46]:

$$q_h = -\Delta H - P_{HT-PEMFC} - q_L - q_{re} = -\frac{A\Delta h}{2F} \left[(1 - \eta_{HT-PEMFC})j - \frac{2F(c_1 + c_2)(T - T_0)}{-\Delta h} \right] \tag{13}$$

where $c_1 = [K_{re}A_{re}(1 - \varepsilon)]/A$ and $c_2 = K_L A_L/A$ are two composite parameters that are related to the geometry configurations and the heat transfer irreversibility of the HT-PEMFC and regenerator.

Due to the existing regenerative losses in the regenerator and heat leakage from the HT-PEMFC to the ambience, the APR begins to absorb heat from the cooled space when $q_h > 0$. Thus, based on Eq. (13), the lower bound of operating current density from which the APR begins to absorb heat from the cooled space j_c is determined by

$$j_c = \frac{2F(c_1 + c_2)(T - T_0)}{-\Delta h(1 - \eta_{HT-PEMFC})} \tag{14}$$

where $\eta_{HT-PEMFC}(j_c)$ is the efficiency of HT-PEMFC at j_c .

When $j > j_c$, the equivalent power output P and efficiency η of the combined system can be, respectively, given by

$$P = P_{HT-PEMFC} + P_{APR} = P_{HT-PEMFC} + \frac{q_h}{2} \left| 1 - \frac{T_0}{T_c} \right| \left\{ \left[\left(a + \frac{I_r T_0 - T_c}{Cq_h} \right)^2 - 4T_c \left(\frac{1}{(1+D)^2 T} - \frac{1 - I_r T_0/T}{Cq_0} \right) \right]^{0.5} - \left[a + \frac{I_r T_0 - T_c}{Cq_h} \right] \right\} \tag{15}$$

and

$$\eta = -\frac{2FP}{j\Delta h} = -\frac{2F}{j\Delta h} \left\{ P_{HT-PEMFC} + \frac{q_h}{2} \left| 1 - \frac{T_0}{T_c} \right| \left\{ \left[\left(a + \frac{I_r T_0 - T_c}{Cq_h} \right)^2 - 4T_c \left(\frac{1}{(1+D)^2 T} - \frac{1 - I_r T_0/T}{Cq_h} \right) \right]^{0.5} - \left[a + \frac{I_r T_0 - T_c}{Cq_h} \right] \right\} \right\} \tag{16}$$

When $j \leq j_c$, the power output P and efficiency η of the combined system equal to that of the sole HT-PEMFC, i.e.,

$$P = P_{HT-PEMFC} \tag{17}$$

and

$$\eta = \eta_{HT-PEMFC} \tag{18}$$

3. RESULTS AND DISCUSSION

Table 1. Parameters used for the modeling.

Parameter	Value
Faraday constant, F (C mol ⁻¹)	96,485
Thickness of the electrolyte, t_{mem} (m)	5×10^{-5} [55]
Universal gas constant, R (J mol ⁻¹ K ⁻¹)	8.314
Number of electrons, n_e	2
Operating temperature, T (K)	433
Temperature of environment, T_0 (K)	313
Temperature of cooled space, T_c (K)	293
Anode pressure (atm)	1.08 [53]
Cathode pressure (atm)	1.28 [53]
Anode gas compositions	100% H ₂
Cathode gas compositions	21% O ₂
Charge transfer coefficient, α	0.5 [35]
Leak current density, j_{leak} (A m ⁻²)	5×10^{-8} [54]
Internal irreversible of absorption refrigerant, I_r	1.05 [51]
The doping level, DL	10
The relative humidity, Rh	3.8%
Polar plate area of the HT-PEMFC, A (m ²)	0.005
Constant, a (W K ⁻¹ m ⁻²)	1 [27]
Constant, b_1 (W K ⁻¹ m ⁻²)	0.9 [47]
Constant, b_2 (W K ⁻¹ m ⁻²)	0.2 [47]
Constant, c_1 (W K ⁻¹ m ⁻²)	0.001 [45]
Constant, c_2 (W K ⁻¹ m ⁻²)	0.001

3.1. Generic performance characteristics

Based on the mathematical model formulated in Section 2 and the typical parameter values in Table 1, the generic performance characteristics of the combined system can be revealed. The curves of equivalent power densities and efficiencies of the HT-PEMFC, APR and combined system varying with the operating current density can be obtained, as shown in Fig. 3, where $P^* = P/A$ is the equivalent power density of the combined system; $P_{HT-PEMFC}^* = P_{HT-PEMFC}/A$ and $P_{APR}^* = P_{APR}/A$ are, respectively, the equivalent power densities of the HT-PEMFC and APR; P_{max}^* , $P_{max,HT-PEMFC}^*$ and $P_{max,APR}^*$ are, respectively, the maximum equivalent power densities of the combined system, HT-PEMFC and APR; η_p ($\eta_{p,HT-PEMFC}$ or $\eta_{p,APR}$) and j_p ($j_{p,HT-PEMFC}$ or $j_{p,APR}$) are the equivalent efficiency and operating current density of the combined system (HT-PEMFC or APR) at P_{max}^* ($P_{max,HT-PEMFC}^*$ or $P_{max,APR}^*$), respectively. It is observed that the equivalent power densities of the HT-PEMFC, APR and combined system first grow and then reduce as j is increased, while their equivalent efficiencies ongoingly

decrease with the increasing j Fig. 3 also shows that j_p , $j_{p,HT-PEMFC}$ and $j_{p,APR}$ are not equal to each other. For the parameters in Table 1, the combined system reaches P_{max}^* , 3976.24 W m⁻², at 13188.52 A m⁻², and the HT-PEMFC reaches $P_{max,HT-PEMFC}^*$, 3694.77 W m⁻², at 13564.56 A m⁻², while the APR reaches $P_{max,APR}^*$, 9955.46 W m⁻², at 310.46 A m⁻². Meanwhile, η_p , $\eta_{p,HT-PEMFC}$ and $\eta_{p,APR}$ are 24%, 21% and 3.5%, respectively. Both the equivalent power density of the combined system and its corresponding efficiency are greater than either that of the HT-PEMFC or that of the APR. It clearly shows that the proposed combined system performance gains obvious improvement by integrating an APR. For the parameters in Table 1, numerical calculations show that the equivalent output power density and efficiency of the combined system are improved by 7.9% and 14.3% in comparison to that of the sole HT-PEMFC, respectively.

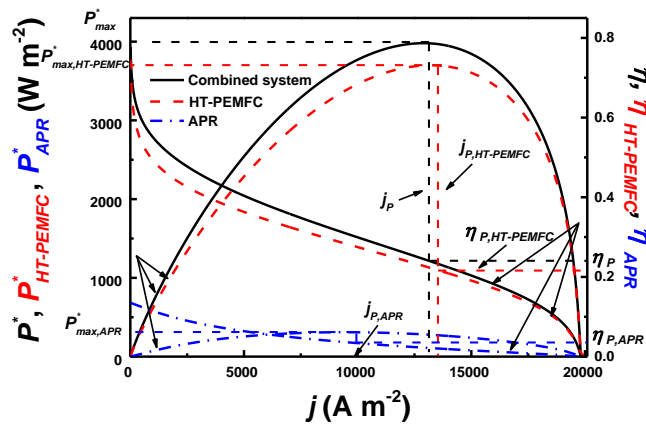


Figure 3. Curves of equivalent power densities and efficiencies for the HT-PEMFC, APR, and combined system varying with the HT-PEMFC operating current density, where $P^* = P/A$ is the equivalent power density of the combined system, $P_{HT-PEMFC}^* = P_{HT-PEMFC}/A$ and $P_{APR}^* = P_{APR}/A$ are, respectively, the power densities of the HT-PEMFC and APR; P_{max}^* , $P_{max,HT-PEMFC}^*$ and $P_{max,APR}^*$ are, respectively, the maximum equivalent power densities of the combined system, HT-PEMFC and APR; j_p is the operating current density of HT-PEMFC at P_{max}^* ; $\eta_{p,HT-PEMFC}$ ($\eta_{p,APR}$) and $j_{p,HT-PEMFC}$ ($j_{p,APR}$) are the equivalent efficiency and operating current density of HT-PEMFC (APR) at $P_{max,HT-PEMFC}^*$ ($P_{max,APR}^*$), respectively.

As illustrated in Fig. 3, both P^* and η reduce with j when $j > j_p$. Obviously, the optimum operation region of j should be

$$j_c < j \leq j_p \tag{19}$$

3.2. Parametric studies

As shown by the established mathematical model, the performance of the combined system not only depends on the phosphoric acid doping level, relative humidity of proton exchange membrane, some comprehensive parameters related to heat-transfer irreversibility and operating temperature but also depends on the proton exchange membrane thickness. In this section, the impacts of these

parameters on the combined system performance will be discussed in detail and the results of this model are compared with the other HT-PEMFC-based hybrid systems.

3.2.1. Effects of DL

DL refers to the number of phosphoric acid molecules around each polybenzimidazole. The PA/PBI membrane can reduce the dependence on water and increase the number of donors and acceptors, and thus a higher DL improves the conductivity of HT-PEMFC as well as the overall performance of the combined system.

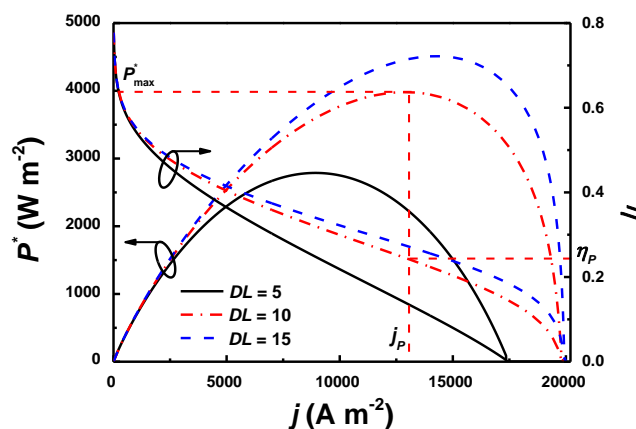


Figure 4. Effect of the doping degree on the equivalent power density and efficiency of the combined system.

As shown in Fig. 4, both P^* and η increase with DL in the whole region of, j and the effects of DL on P^* and η become insusceptible as DL increases. In addition, both j_{P^*} and P^*_{max} shift to larger values as DL increases. Although a larger DL benefits the system performance improvement, the mechanical strength of PA/PBI membrane becomes weaker at the same time.

3.2.2. Effects of Rh

Rh is another parameter that affects the conductivity of proton exchange membrane for HT-PEMFC and therefore affects the ohmic overpotential of the HT-PEMFC. Thus, Rh is crucial to the HT-PEMFC performance as well as the combined system performance. As shown in the Fig. 5, the influence of Rh on P^* and η is obvious when j is between 5000 A m^{-2} and 20000 A m^{-2} . When j is less than 5000 A m^{-2} , Rh has almost no influence on the system performance.

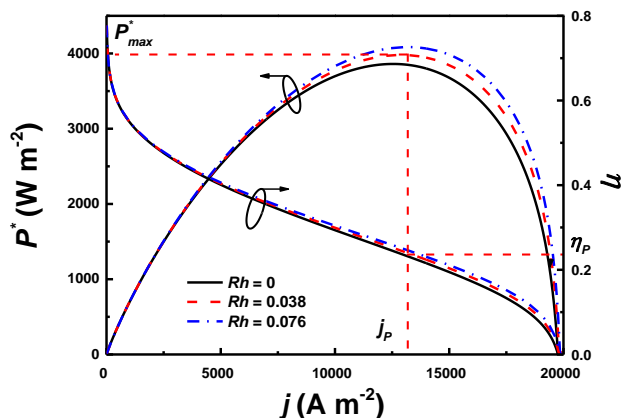


Figure 5. Effect of the humidity on the equivalent power density and efficiency of the combined system. Numerical calculations show that P_{max}^* increases from 3869.15 W m^{-2} to 4106.83 W m^{-2} when Rh grows from 0 to 7.6%, while η_p and j_p are almost unchanged. In recent years, researchers are dedicated to reducing the design complexity and additional power for the inlet gas humidification.

3.2.3. Effects of b_1

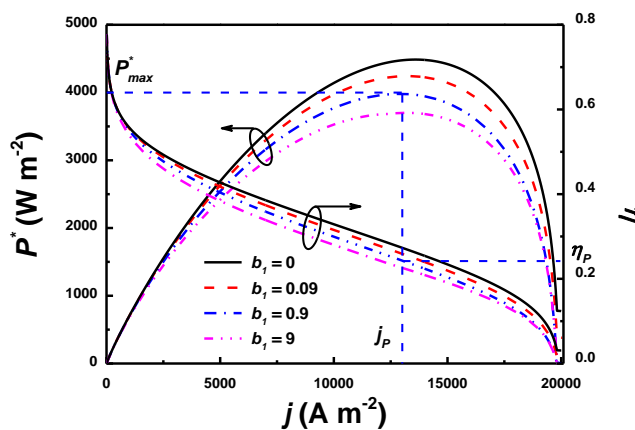


Figure 6. Effect of the integrated parameter b_1 on the equivalent power density and efficiency of the combined system.

$b_1 = K_h/K_0$ is a composite parameter that is closely related to the heat transfer irreversibility. It can be seen from Fig. 6 that both P^* and η of the combined system are monotonically decreased with b_1 , and P_{max}^* and η_p of the combined system are slightly reduced as b_1 increases. However, j_p remains almost unchanged when b_1 changes. The black solid lines in Fig. 6 stands for the special case that the heat-transfer irreversible losses between the environment and condenser or absorber are negligibly small.

3.2.4. Effects of b_2

$b_2 = K_h/K_c$ is another composite parameter that significantly affect the APR performance. Similar to b_1 , the heat-transfer irreversible losses between the evaporator and the cooled space decrease as b_2 decreases. As shown in the Fig. 7, both P^* and η are also monotonically decreasing functions of b_2 , and P^*_{max} decreases as b_2 increases while j_p and η_p are almost constants. In addition, the effects of b_2 on P^* and η become insusceptible as b_2 decreases. The black solid lines in Fig. 7 stand for the special case that the heat-transfer irreversible losses between the evaporator and the cooled space are negligibly small.

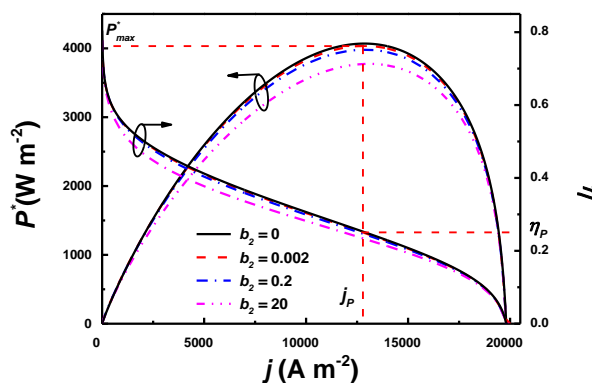
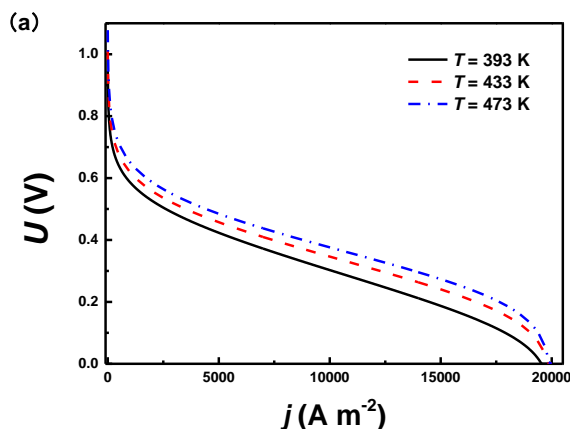


Figure 7. Effect of the integrated parameter b_2 on the equivalent power density and efficiency of the combined system.

3.2.5. Effects of T

The HT-PEMFC operating temperature T is a key operating condition that affects the HT-PEMFC performance as well as the APR performance. As seen from Eqs. (3) - (6), T mainly affects E_0 , E_{act} , E_{con} and E_{ohm} and thus impacts U . It is observed from Fig. 8. (a) that increases with the increase of T .



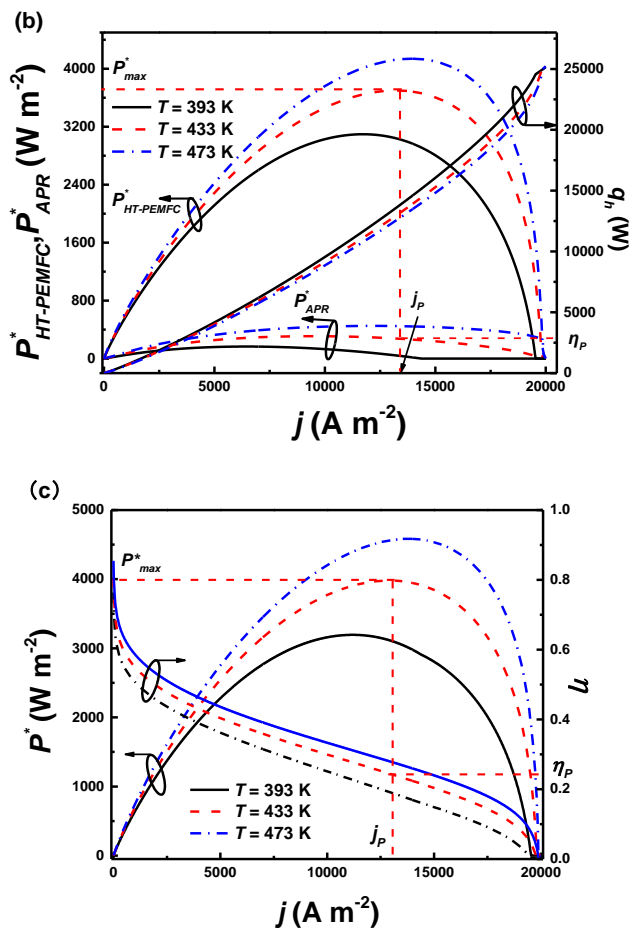


Figure 8. Effect of the operating temperature on (a) output voltage of HT-PEMFC, (b) the heat flowing from HT-PEMFC to environment, equivalent output power density of HT-PEMFC and APR, and (c) the equivalent power density and efficiency of the combined system.

Therefore, a higher T is beneficial for HT-PEMFC performance improvement, as shown in Fig. 8 (b). Besides, the temperature difference ($T - T_0$) between HT-PEMFC and the environment is increased as T rises, which creates a bigger q_h and improves the performance of APR as shown in Fig. 8 (b). In general, an increasing T is beneficial for the performance improvement of the combined system, as shown in Fig. 8 (c). Fig. 8 (c) also shows that both P^*_{max} and η_p are improved with increasing T . Meanwhile, j_p gradually moves rightward. When $T = 393$ K, P^*_{max} , η_p and j_p are 3200.77 W m⁻², 22.6% and 11086.31 A m⁻², respectively. When $T = 433$ K, P^*_{max} , η_p and j_p are 3987.24 W m⁻², 23.8% and 13115.29 A m⁻², respectively. When $T = 473$ K, P^*_{max} , η_p and j_p are 4610.90 W m⁻², 24.2% and 14066.93 A m⁻², respectively.

3.2.6. Effects of t_{mem}

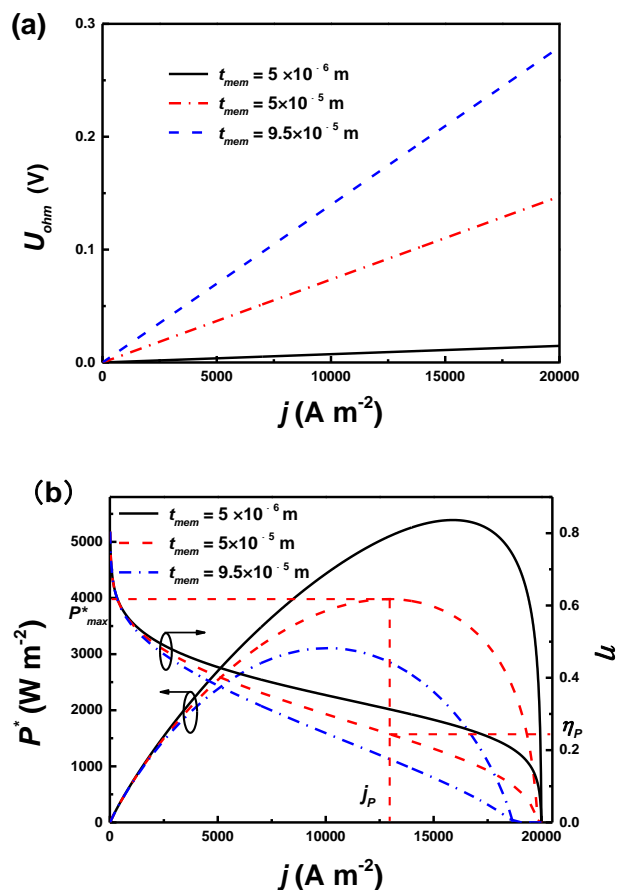


Figure 9. Effect of the proton exchange membrane thickness on (a) the ohm overpotential of HT-PEMFC, and (b) equivalent power density and efficiency of the combined system.

The thickness of the electrolyte t_{mem} has a great influence on the performance of the fuel cell. As illustrated in Fig. 9 (a), a higher t_{mem} greatly increases the HT-PEMFC ohm overpotential E_{ohm} . This is because the larger electrolyte thickness increases the impedance of the ions transport, which affects the power output of HT-PEMFC as well as the equivalent output power density and efficiency of the combined system. It can be seen from Fig. 9 (b) that both P^* and η are monotonically decreasing functions of t_{mem} . In addition, P^*_{max} and η_P are greatly reduced with t_{mem} .

3.2.7. Model comparison

To further verify the correctness and validity of the HT-PEMFC and APR combined system model presented here. We compared the maximum power densities at different temperatures with the Guo's HT-PEMFC combined system where the bottoming cycle can be functioned as either an absorption heat pump for heating or an absorption refrigerator for cooling hybrid system [56] and Lee's HT-PEFC combined system where an APR was integrated [33], as depicted in Fig. 10. From Fig. 10, we can see that the maximum output power densities of the three systems increase with the increase of temperature

in the range of 423~473 K. The present combined system maximum power density is almost the same as that of Lee' model [33], while it is smaller than that of the Guo's model. This is because Guo's absorption refrigerator model did not consider the internal irreversible losses inside the working fluid. The results show that the proposed combined system model is reliable and can be regarded as an effective way to enhance the HT-PEMFC performance.

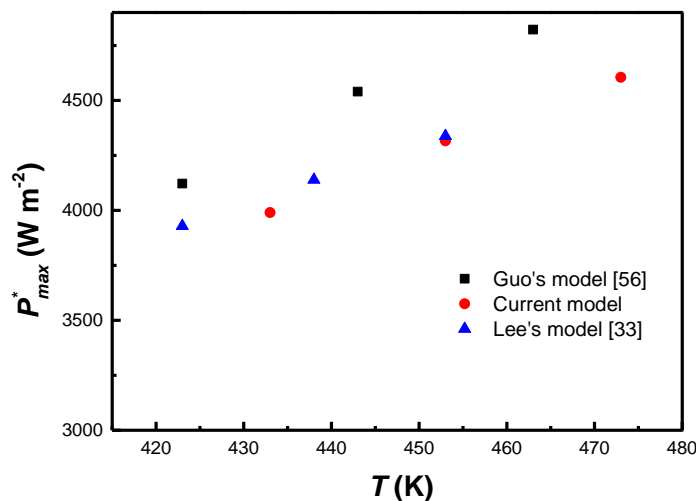


Figure 10. Maximum power density comparisons between the present combined system and the Guo's combined system [56] and Lee's combined system [33].

4. CONCLUSIONS

In order to reuse the waste heat of HT-PEMFC, an APR is integrated with the fuel cell for cooling production. By considering the existing thermodynamic-electrochemical irreversible losses within the combined system, the equivalent power output and efficiency of the HT-PEMFC, the APR and the proposed system are calculated. The generic performance characteristics and optimum ranges of the operating current density are derived. Compared with the single HT-PEMFC, the maximum equivalent output power density and its corresponding efficiency for the combined system are increased by 7.9% and 14.3% respectively. The effects of the operating temperature, operating current density and proton exchange membrane thickness, phosphoric acid doping level, relative humidity of HT-PEMFC, and some crucial composite parameters related to thermodynamic losses on the combined system performance are discussed. The obtained results are useful for the integration and design of an actual combined system.

ACKNOWLEDGEMENTS

This work has been supported by the K. C. Wong Magna Fund in Ningbo University.

References

1. J.H. Wee, *Renew. Sust. Energ. Rev.*, 11 (2007) 1720.
2. A. Kirubakaran, S. Jain and R.K. Nema, *Renew. Sust. Energ. Rev.*, 13 (2009) 2430.
3. Y. Wang, K.S. Chen, J. Mishler, S.C. Cho and X.C. Adroher, *Appl. Energy*, 88 (2011) 981.
4. M.Y. El-Sharkh, A. Rahman, M.S. Alam, P.C. Byrne, A.A. Sakla and T. Thomas, *J. Power Sources*, 138 (2004) 199.
5. J.J. Hwang, M.L. Zou, W.R. Chang, A. Su, F.B. Weng and W. Wu, *Int. J. Hydrogen Energy*, 35 (2010) 8644.
6. P. Yang and H. Zhang, *Energy*, 85 (2015) 458.
7. A.H. Mamaghani, B. Najafi, A. Casalegno and F. Rinaldi, *J. Clean. Prod.*, 180 (2018) 126.
8. M. Rahimi-Esbo, A. Ramiar, A.A. Ranjbar and E. Alizadeh, *Int. J. Hydrogen Energy*, 42 (2017) 11673.
9. T.J. Omasta, A.M. Park, J.M. Lamanna, Y. Zhang, X. Peng, L. Wang, D.L. Jacobson, J.R. Varcoe, D.S. Hussey, B.S. Pivovarc and W.E. Mustain, *Energ. Environ. Sci.*, 11 (2018) 551.
10. U.U. Ince, H. Markötter, M.G. George, H. Liu, N. Ge, J. Lee, S.S. Alrwashdeh, R. Zeis, M. Messerschmidt, J. Scholta, A. Bazylak and I. Mankea, *Int. J. Hydrogen Energy*, 43 (2018) 391.
11. S. Authayanun, M. Mamlouk, K. Scott and A. Arpornwichanop, *Appl. Energy*, 109 (2013) 192.
12. Y. Liu, W. Lehnert, H. Janßen, R.C. Samsun and D. Stolten, *J. Power Sources*, 311 (2016) 91.
13. T.J. Bvumbe, P. Bujlo, I. Tolj, K. Mouton, G. Swart, S. Pasupathi and B.G. Pollt, *Hydrogen and Fuel Cells*, 1 (2016) 1.
14. Q. Zhang, L. Xu, J. Li and M. Ouyang, *Int. J. Hydrogen Energy*, 43 (2018) 1736.
15. V. Liso, M.P. Nielsen, S.K. Kær and H.H. Mortensen, *Int. J. Hydrogen Energy*, 39 (2014) 8410.
16. P. Lettenmeier, W. Li, U. Golla-Schindler, P. Gazdzicki, N.A. Cañas, M. Handl, R. Hiesgen, S.S. Hosseing, A.S. Gago and K.A. Friedrich, *Angew. Chem.*, 128 (2016) 752.
17. A. Arsalis, S.K. Kær and M.P. Nielsen, *Appl. Energy*, 147 (2015) 569.
18. G.H. Kim, K.S. Eom, M.G. Kim, S.J. Yoo, J.H. Jang, H. Kim and E.A. Cho, *ACS Appl. Mater. Inter.*, 7 (2015) 27581.
19. A. Brouzgou, S.Q. Song and P. Tsiakaras, *Appl. Catal. B-Environ.*, 127 (2012) 371.
20. S.J. Peighambaroust, S. Rowshanzamir and M. Amjadi, *Int. J. Hydrogen Energy*, 35 (2010) 9349.
21. H. Zhang and P.K. Shen, *Chem. Rev.*, 112 (2012) 2780.
22. A. Perna, M. Minutillo and E. Jannelli, *Energy*, 88 (2015) 874.
23. N. Sarabchi, S.M.S. Mahmoudi, M. Yari and A. Farzi, *Energ. Convers. Manage.*, 190 (2019) 14.
24. L. Chen, T. Zheng, F. Sun and C. Wu, *Sol. Energy*, 03 (2004) 347.
25. I. Pilatowsky, R.J. Romero, C.A. Isaza, S.A. Gamboa, W. Rivera, P.J. Sebastian and J. Moreira, *Int. J. Hydrogen Energy*, 32 (2007) 3174.
26. A. Arsalis, S.K. Kaer and M.P. Nielsen, *Appl. Energy*, 147 (2015) 569.
27. J.J. Hwang and M.L. Zou, *J. Power Sources*, 195 (2010) 2579.
28. A. Colmenar-Santos, L. Alberdi-Jimenez, L. Nasarre-Cortes and J. Mora-Larramona, *Energy*, 68 (2014) 182.
29. P. Zhao, J. Wang, L. Gao and Y. Dai, *Int. J. Hydrogen Energy*, 37 (2012) 3382.
30. D. Borello, Z.D. Prete, A. Marchegiani, F. Rispoli and E. Tortora, In: ASME turbo expo; turbine technical conference and exposition. *Denmark*. June 3 (2012) 11.
31. M.A. Gadalla and T.A.H. Ratlamwala, *Int. J. Exergy*, 7 (2010) 731.
32. T.A.H. Ratlamwala, M.A. Gadalla and I. Dincer, *Fuel Cells*, 11 (2011) 413.
33. W.Y. Lee, M. Kim, Y.J. Sohn and S.G. Kim, *Energy*, 141 (2017) 2397.
34. X. Gao, S.J. Andreasen, S.K. Kær and L.A. Rosendahl, *Int. J. Hydrogen Energy*, 12 (2014) 6637.
35. J. Zhang, L. Song, S.H. Pedersen, H. Yin and L.T. Hung, *Nat. Commun.*, 8 (2017) 13901.
36. A. Kodal, B. Sahin, I. Ekmekci and T. Yilmaz, *Energ. Convers. Manage.*, 44 (2003) 109.
37. J. Chen and J.A. Schouten, *Energ. Convers. Manage.*, 39 (1998) 999.

38. P.A.N. Wouagfack and R. Tchinda, *Int. J. Refrig.*, 34 (2011) 1008.
39. B.A.M. Nouadje, P.A.N. Wouagfack and R. Tchinda, *Int. J. Refrig.*, 38 (2014) 118.
40. M. Ay, A. Midilli and I. Dincer, *Int. J. Energ. Res.*, 30 (2006) 307.
41. M.G. Santarelli, M.F. Torchio and P. Cochis, *J. Power Sources*, 159 (2006) 824.
42. P.A.N. Wouagfack and R. Tchinda, *Int. J. Refrig.*, 40 (2014) 404.
43. M.H. Ahmadi and M.A. Ahmadi, *Renew. Sust. Energ. Rev.*, 60 (2016) 784.
44. J. Brouwer, F. Jabban, E.M. Leal and T. Orr, *J. Power Sources*, 158 (2006) 213.
45. H. Zhang, G. Lin and J. Chen, *Int. J. Electrochem. Sc.*, 6 (2011) 714.
46. S.O. Mert, I. Dincer and Z. Ozcelik, *J. Power Sources*, 165 (2007) 244.
47. X. Zhang, J. Guo and J. Chen, *Energy*, 35 (2010) 5294.
48. J. Nieminen, I. Dincer and G. Naterer, *Int. J. Hydrogen Energy*, 35 (2010) 10842.
49. T.E. Springer, T.A. Zawodzinski and S. Gottesfeld, *Int. J. Electrochem. Sc.*, 138 (1991) 2334.
50. S. Authayanun and V. Hacker, *Energ. Convers. Manage.*, 160 (2018) 230.
51. G. Lin and Z. Yan, *J. Phys. D: Appl. Phys.*, 32 (1999) 94.
52. X. Qin, L. Chen, Y. Ge and F. Sun, *Arab. J. Sci. Eng.*, 38 (2013) 405.
53. X. Zhang, X. Chen, B. Lin and J. Chen, *Int. J. Hydrogen Energy*, 36 (2011) 2190.
54. X. Chen, Y. Wang and Y. Zhou, *Int. J. Elec. Power*, 63 (2014) 429.
55. P.O. Olapade, J.P. Meyers, B.L. Borup and R. Mukundan, *J. Electrochem. Soc.*, 158 (2011) 639.
56. X. Guo, H. Zhang, J. Zhao, F. Wang, J. Wang, H. Miao and J. Yuan, *Energ. Convers. Manage.*, 181 (2019) 292.

© 2019 The Authors. Published by ESG (www.electrochemsci.org). This article is an open access article distributed under the terms and conditions of the Creative Commons Attribution license (<http://creativecommons.org/licenses/by/4.0/>).